Molecular Structures and Ion Mobility Cross Sections: Analysis of the Effects of He and N_2 Buffer Gas

Christian Bleiholder[†], Nicholas R. Johnson[‡], Stephanie Contreras[±], Thomas Wyttenbach, and Michael T. Bowers*

Department of Chemistry and Biochemistry, University of California Santa Barbara, Santa Barbara, California 93106, United States.

AUTHOR INFORMATION

Corresponding Author

Michael T. Bowers

bowers@chem.ucsb.edu

Present Addresses

†Department of Chemistry & Biochemistry and Institute of Molecular Biophysics, Florida State University, Tallahassee, FL 32306-4390

‡Department of Chemistry & Biochemistry, University of Colorado at Boulder, Boulder, CO, 80309

±Department of Chemistry, University of California at Davis, One Shields Ave, Davis, CA 95616

SUPPORTING INFORMATION

1 Experimental and computed collision cross sections

Table S1. Cross section data for tetraglycine

Helium						Nitrogen					
Experiment		PSA Cross Section				Experiment		PSA Cross Section			
T	CCS	T	PA	RHO	PSA	T	CCS	T	PA	RHO	PSA
77.6	120.9	80.0	110.2	1.0	110.9	77.5	355.6	80.0	361.0	1.0	362.1
77.6	121.7	120.0	97.0	1.0	98.9	77.5	356.0	120.0	262.5	1.0	263.8
124.1	100.7	150.0	91.2	1.0	92.9	77.6	359.1	150.0	223.3	1.0	224.2
127.2	98.9	220.0	83.1	1.0	85.0	97.1	302.1	220.0	176.3	1.0	177.0
169.7	97.0	300.0	77.9	1.0	79.0	98.6	300.4	300.0	142.1	1.0	143.1
170.5	95.4	400.0	74.0	1.0	74.5	152.8	217.9	400.0	120.2	1.0	120.3
250.9	85.7	600.0	70.0	1.0	71.5	152.9	219.7	600.0	97.7	1.0	98.0
251.7	85.6					153.2	219.9				
299.1	83.0					180.1	210.8				
299.1	83.2					180.9	211.2				
398.2	79.1					181.0	208.7				
398.3	78.6					236.6	171.5				
493.9	78.1					237.6	171.9				
494.1	78.6					238.7	174.2				
						299.3	155.1				
						299.3	154.3				
						299.3	155.3				
						301.6	153.2				
						350.7	137.3				
						351.1	139.5				
						351.6	137.3				
						420.2	129.3				
						420.7	129.5				
						457.5	125.0				
						467.9	122.1				
						467.9	123.0				
						551.0	120.7				
						551.1	120.3				
						551.4	110.7				

Table S2. Cross section data for potassiated 18-Crown-6

Helium						Nitrogen					
Experiment		PSA Cross Section				Experiment		PSA Cross Section			
T	CCS	T	PA	RHO	PSA	T	CCS	T	PA	RHO	PSA
77.5	140.8	80.0	133.2	1.0	135.2	77.7	352.5	80.0	327.6	1.0	327.8
77.6	139.1	120.0	119.7	1.0	122.2	77.7	352.5	120.0	249.9	1.0	251.1
116.9	121.5	150.0	113.6	1.0	115.3	78.1	340.5	150.0	218.1	1.0	218.6
120.4	122.2	220.0	105.1	1.0	107.1	78.5	354.5	220.0	177.4	1.0	178.4
172.0	113.0	300.0	99.7	1.0	100.6	79.7	357.0	300.0	152.9	1.0	153.8
174.3	112.7	400.0	95.4	1.0	97.1	106.6	286.3	400.0	136.3	1.0	137.7
252.1	105.2	600.0	90.7	1.0	91.0	107.5	282.9	600.0	120.7	1.0	121.6
254.3	105.4					107.7	284.3				
298.7	101.1					155.2	214.7				
298.8	101.5					155.6	221.3				
344.6	99.7					155.6	220.0				
344.8	99.4					196.6	203.5				
398.2	97.6					196.8	203.1				
398.3	97.1					197.0	203.6				
496.7	94.5					231.7	184.0				
497.5	94.3					234.0	177.0				
						234.9	176.5				
						299.6	161.7				
						299.6	161.9				
						299.6	160.7				
						352.8	149.5				
						352.8	149.5				
						353.1	148.5				
						353.2	149.3				
						354.8	150.0				
						359.8	150.6				
						364.8	151.6				
						369.8	152.7				
						420.3	139.0				
						420.4	138.6				
						420.5	138.4				
						467.6	133.7				
						467.6	133.6				
						467.6	133.6				
						467.8	132.5				
						469.6	133.9				
						472.6	134.3				
						477.6	135.1				
						482.6	135.8				
						549.9	126.5				
						550.0	125.0				
						550.1	123.4				

Table S3. Cross section data for sodiated 18-Crown-6

Helium						Nitrogen					
Experiment		PSA Cross Section				Experiment		PSA Cross Section			
T	CCS	T	PA	RHO	PSA	T	CCS	T	PA	RHO	PSA
254.2	99.4	80.0	126.4	1.0	131.0	77.5	336.7	80.0	321.4	1.0	324.5
252.6	99.5	120.0	113.1	1.0	117.1	77.5	336.7	120.0	243.8	1.0	246.8
298.7	96.4	150.0	106.9	1.0	111.3	77.5	336.9	150.0	210.3	1.0	214.0
298.8	96.2	220.0	98.2	1.0	102.9	77.6	336.8	220.0	170.4	1.0	172.9
344.5	95.7	300.0	92.8	1.0	97.3	105.0	280.4	300.0	147.2	1.0	149.5
344.7	95.5	400.0	88.5	1.0	92.5	105.4	282.0	400.0	132.4	1.0	134.7
398.4	93.2	600.0	83.8	1.1	88.0	105.7	282.3	600.0	116.7	1.0	119.1
398.2	93.7					153.0	209.4				
498.5	92.4					153.0	211.6				
496.9	91.7					153.2	211.9				
116.0	115.2					190.6	200.1				
119.2	115.0					191.1	201.0				
173.2	106.8					192.0	200.8				
175.1	105.1					228.5	176.9				
77.5	132.6					228.8	178.0				
77.6	132.7					228.9	177.2				
						299.3	156.7				
						299.3	156.9				
						299.3	157.5				
						301.6	157.0				
						352.2	143.2				
						352.4	144.8				
						352.4	144.8				
						352.7	145.1				
						354.4	145.2				
						357.4	145.8				
						362.4	146.8				
						367.4	147.8				
						420.7	135.1				
						420.7	135.0				
						420.7	133.4				
						457.0	129.9				
						467.7	130.0				
						467.8	130.2				
						467.8	130.2				
						467.9	131.3				
						469.8	130.5				
						472.8	130.9				
						477.8	131.6				

(still experimental)	
T	CCS
482.8	132.3
550.1	122.8
550.9	122.6
550.0	122.0

Table S4. Cross section data for protonated ubiquitin.

	N-state		broad peak		A-state	
z	He	N_2	He	N_2	He	N_2
6	970	1200				
6				1380		
7	1000	1270				
7			1250	1540		
8	1020	1300				
8			1400	1670		
8					1630	1980
9			1520			
10			1580	1950		
10					1710	2130
10					1760	2170
11			1710	2260		
11					1800	2300
11					1870	2360
12					1920	2470
13					2020	2660

Table S5. Cross section data predicted for protonated ubiquitin by the PSA method.

		Temperature [K]	PA [Å^2]	ρ	PSA [Å^2]
N-State	Helium	80	956.8	1.175	1124.6
		120	909.9	1.180	1073.6
		150	889.2	1.187	1055.7
		230	858.0	1.186	1017.2
		300	843.2	1.196	1008.1
		400	829.2	1.201	995.4
		600	813.0	1.221	992.7
	Nitrogen	80	1869.8	1.099	2054.3
		120	1491.0	1.113	1659.4
		150	1339.5	1.127	1509.8
		230	1145.1	1.138	1302.7
		300	1059.2	1.142	1209.3
		400	989.1	1.149	1136.1
		600	916.5	1.149	1053.5
A-State	Helium	80	1603.1	1.125	1803
		120	1514.4	1.126	1705.9
		150	1473.7	1.134	1671.2
		230	1410.6	1.137	1603.6
		300	1379.0	1.136	1566.1
		400	1351.1	1.142	1543.5
		600	1320.0	1.153	1522.4
	Nitrogen	80	3260.0	1.078	3513.4
		120	2684.6	1.087	2917.8
		150	2438.4	1.092	2661.8
		230	2084.6	1.097	2285.9
		300	1921.6	1.101	2115.9
		400	1785.1	1.108	1977.7
		600	1639.7	1.115	1828.7

Table S6. Cross section data determined on the low-resolution ESI instrument (CCS) and by PSA calculations.

		Temperature [K]	CCS [Å^2] [a]	PSA [Å^2] [b]
Helium	bradykinin	300	243.0	
	angiotensin2	300	253.0	
	melittin	300	589.0	
	1KBK	300		3729
	1JBC	300		5712
	1N9E	300		8451
Nitrogen	bradykinin	300	348.0	
	angiotensin2	300	355.0	
	melittin	300	770.0	
	1KBK	300		4072
	1JBC	300		6181
	1N9E	300		8867

[a] experimental cross sections obtained on the low-resolution instrument
[b] predicted cross sections by the PSA method based on the indicated PDB entry

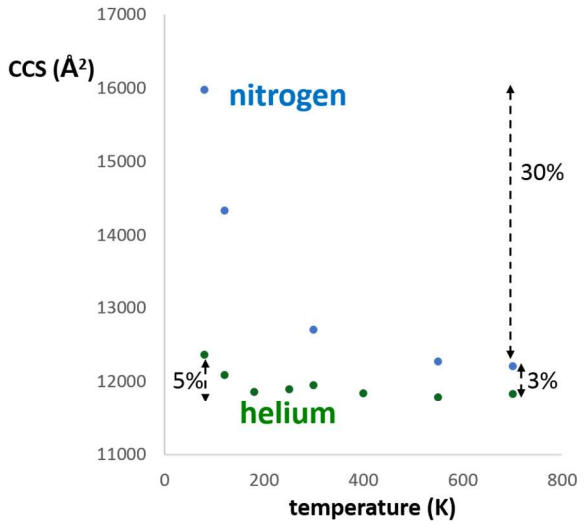

Figure S1. Cross section data predicted by the PSA method for the crystal structure (1OZG) of Klebsiella pneumonia acetolactate synthase in the temperature range from 80 to 700 K. The nitrogen and helium cross sections are predicted to increase by approximately 30% and 5%, respectively, when decreasing the temperature from 700 K to 80 K. A difference between helium and nitrogen cross sections of 3% is noted at 700K.

2 Comparison of helium and nitrogen cross sections to an ideal hard-sphere model.

The hard-sphere collision cross section of a sphere with radius r_0 in a buffer gas with van der Waals radius r_{gas} is given by

$$\Omega_{\text{gas}}(r_0) = \pi \cdot \left(r_0 + r_{gas}\right)^2 = \pi \cdot {R_{gas}}^2$$

where $r_0 + r_{gas} = R_{gas}$.

Thus, the relative increase in cross sections determined in nitrogen and helium buffer gas $\frac{\Omega_{N_2}(r_0) - \Omega_{\text{He}}(r_0)}{\Omega_{\text{He}}(r_0)}$ for a sphere with radius r_0 can be expressed as

$$\frac{\Omega_{N_2}(r_0) - \Omega_{\text{He}}(r_0)}{\Omega_{\text{He}}(r_0)} = \frac{\pi \cdot \left(r_0 + r_{N_2}\right)^2 - \Omega_{\text{He}}}{\Omega_{\text{He}}} = \frac{\pi \cdot \left(R_{\text{He}} + \left(r_{N_2} - r_{\text{He}}\right)\right)^2 - \Omega_{\text{He}}}{\Omega_{\text{He}}} = \frac{\pi \cdot (R_{\text{He}} + \delta R)^2 - \Omega_{\text{He}}}{\Omega_{\text{He}}}$$
$$= \frac{\pi \cdot ({R_{\text{He}}}^2 + 2 \cdot R_{\text{He}} \cdot \delta R + \delta R^2) - \Omega_{\text{He}}}{\Omega_{\text{He}}} = \frac{\pi \cdot (2 \cdot R_{\text{He}} \cdot \delta R + \delta R^2)}{\Omega_{\text{He}}} = \frac{2\sqrt{\pi} \cdot \delta R}{\sqrt{\Omega_{\text{He}}}} + \frac{\pi \cdot \delta R^2}{\Omega_{\text{He}}}$$

Thus,

$$\frac{\Omega_{N_2} - \Omega_{\text{He}}}{\Omega_{\text{He}}} = \frac{2\sqrt{\pi} \cdot \delta R}{\sqrt{\Omega_{\text{He}}}} + \frac{\pi \cdot \delta R^2}{\Omega_{\text{He}}}$$

for spherical hard-sphere ions where $\delta R = r_{N_2} - r_{\text{He}}$ is the difference in van-der Waals radius between nitrogen and helium.

For molecules with globular shapes, we expect the functional dependence on Ω_{He} to be similar but due to molecular roughness and also because the hard-sphere model is known to not be a realistic approximation for the collision process in ion mobility spectrometry, we replace the difference δR by an effective difference in van-der Waals radius δR_{eff}. The value for δR_{eff} can be obtained from plotting $\frac{\Omega_{N_2} - \Omega_{\text{He}}}{\Omega_{\text{He}}}$ as a function of Ω_{He}

Equation S1

$$\frac{\Omega_{N_2} - \Omega_{\text{He}}}{\Omega_{\text{He}}} = \frac{2\sqrt{\pi} \cdot \delta R_{\text{eff}}}{\sqrt{\Omega_{\text{He}}}} + \frac{\pi \cdot {\delta R_{\text{eff}}}^2}{\Omega_{\text{He}}}$$

The value $\delta R_{\text{eff}} = 1.93$ Å fits the recorded and computed data well (Figure S2), indicating that our study determines the radius of nitrogen r_{N_2} to be effectively 1.93 Å larger than the helium radius r_{He}.

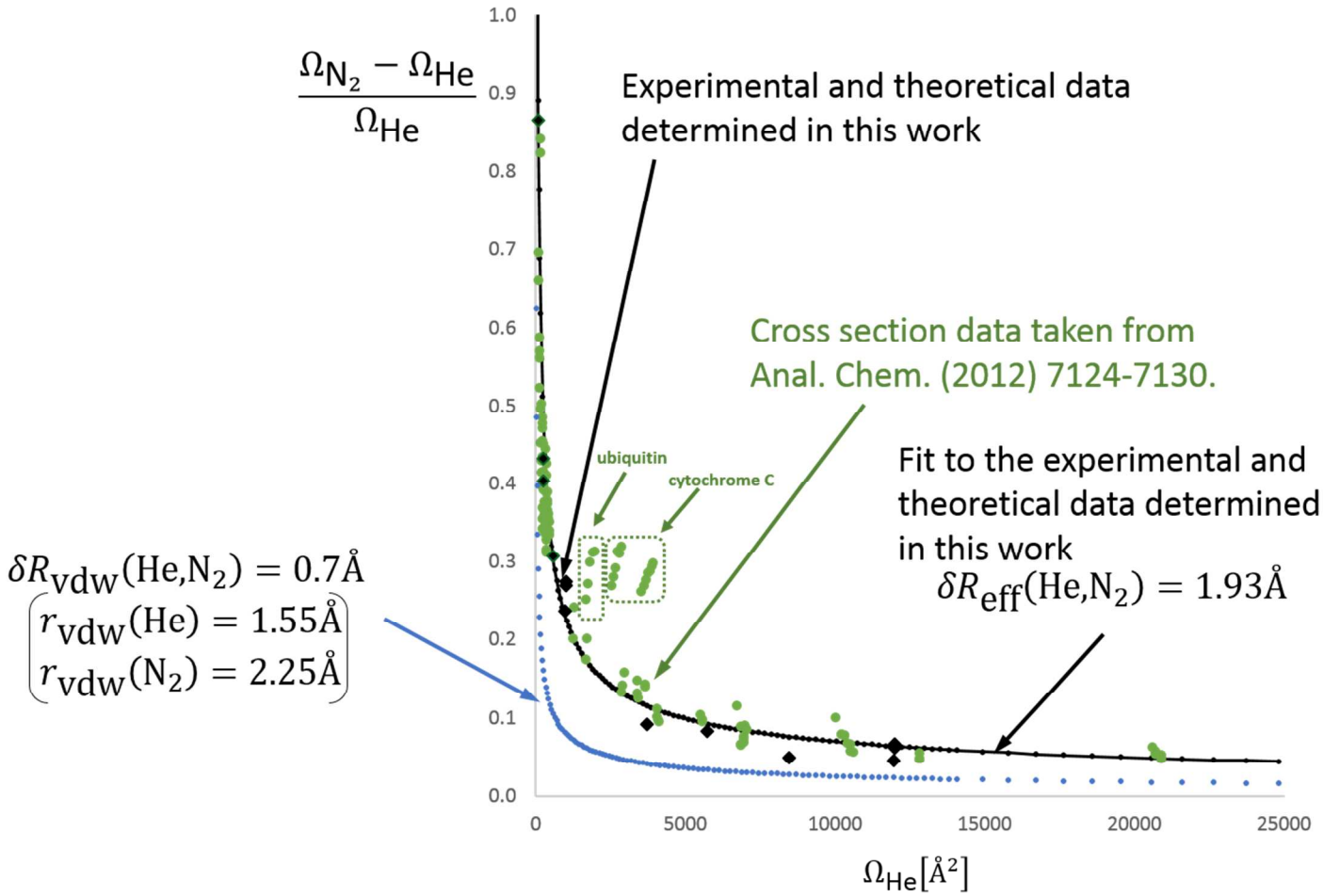

Figure S2. Relative increase in cross sections determined in nitrogen and helium buffer gas $\frac{\Omega_{N_2}-\Omega_{He}}{\Omega_{He}}$ as a function of the helium cross section Ω_{He}. The blue dots represent the correlation for the ideal hard-spheres with $\Omega_{N_2,He}(r_0) = \pi \cdot (r_0 + r_{vdw})^2$ where r_{vdw} is the van-der Waals radius of nitrogen and helium, respectively. Published values of $r_{vdw}(He) = 1.55Å$ and $r_{vdw}(N_2) = 2.25Å$ were used. The black diamonds indicate the experimental and theoretical data obtained in this work (excluding the ubiquitin A-state). These data points were used to fit the effective difference in van der Waals radius δR_{eff} in equation S1 to $\delta R_{eff} = 1.93$ Å (black line). Previously reported cross sections for a number of protein systems were taken from Bush et al., Anal. Chem. (2012) 7124-7130 (green dots). With the exceptions of higher charge states of ubiquitin and cytochrome C, the reported cross sections fit well with the ideal hard-sphere model developed in this work.

3 Structural models used for the PSA calculations

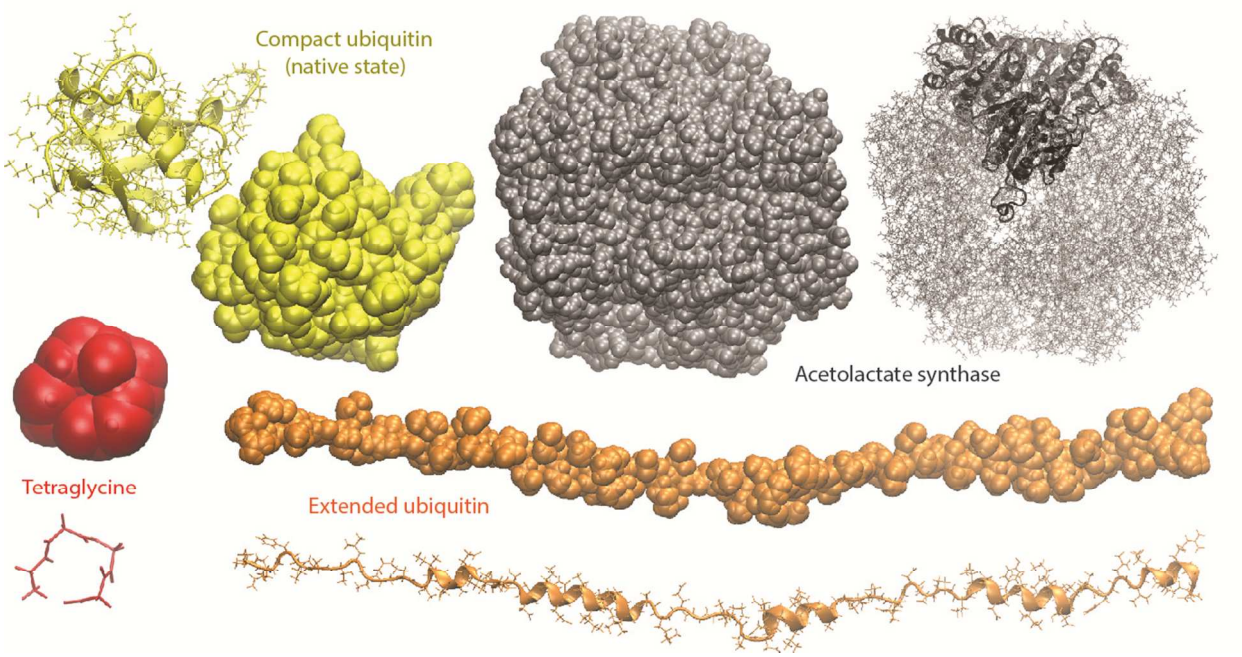

Figure S3. Structural models used in this work for Gly_4H^+, ubiquitin N-state, and acetolactate synthase. Two renderings of an identical geometry in an identical orientation are shown for each molecule, a space-filling representation and a stick model. For ubiquitin and one monomer of acetolactate synthase, the polymer backbone and the secondary structure elements are high-lighted in the stick model. The figure illustrates that the red, yellow, and gray models are globular (quasi-spherical) and that the orange geometry strongly deviates from an overall spherical shape.

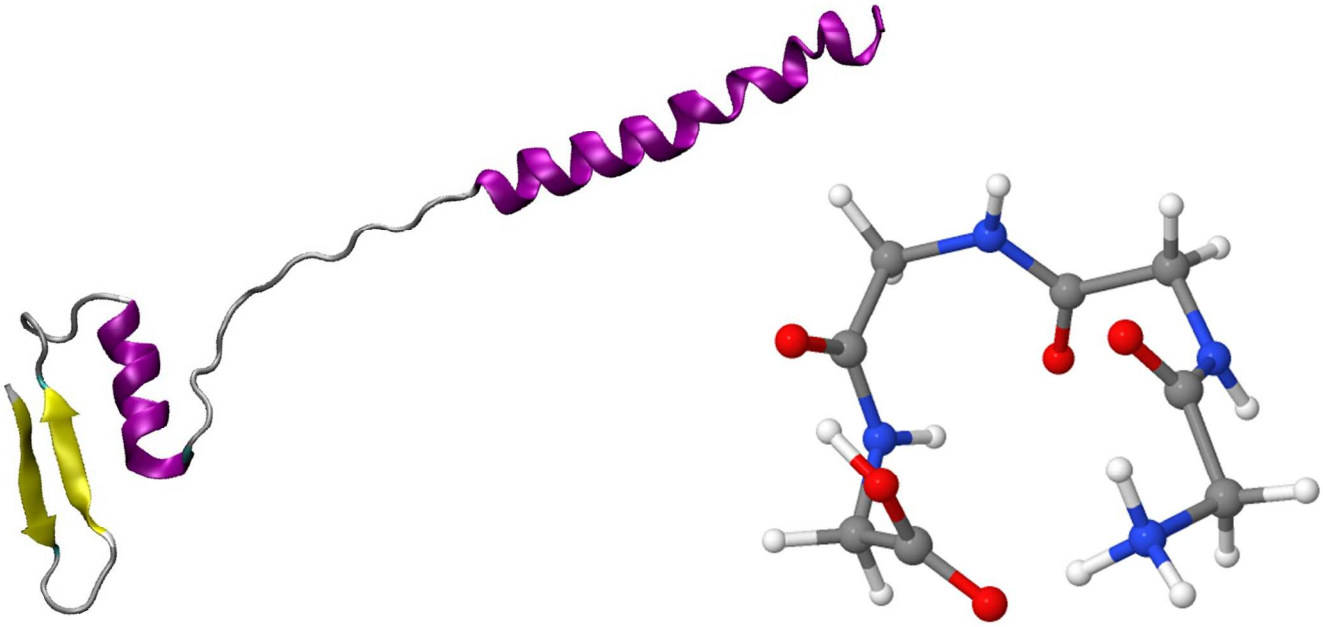

Figure S4. Structural models for the ubiquitin A-state (left) and compact Gly_4H^+ (right). Secondary structural elements and the elemental composition are highlighted in the ubiquitin and in the B3LYP/6-31+G** optimized Gly_4H^+ structure, respectively. The charged N-terminal NH_3 moiety in Gly_4H^+ forms a strong hydrogen bond with the C-terminal carboxylic acid group.

4 Properties of the interaction between two particles

4.1 Carbon-helium versus carbon-nitrogen interaction.

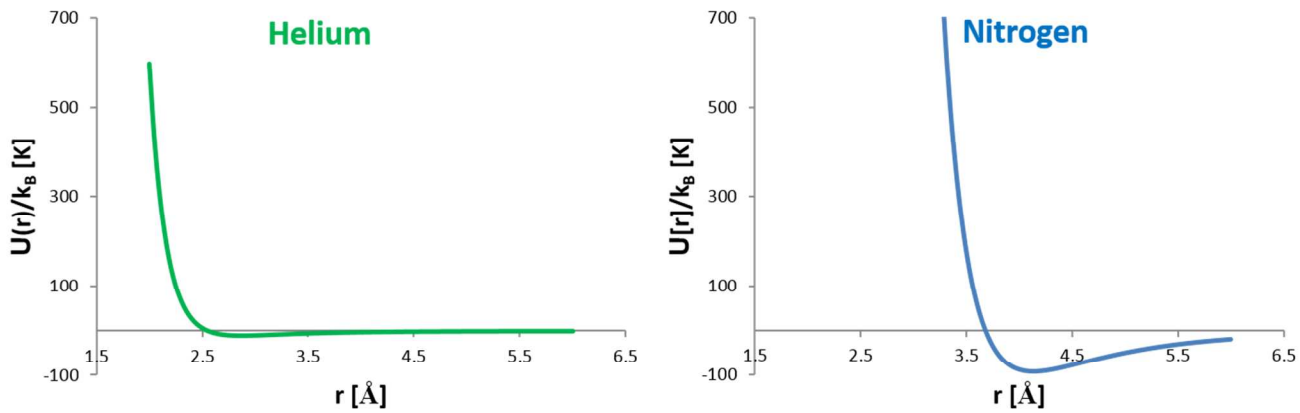

Figure S5: Lennard-Jones interaction potentials for helium and nitrogen with carbon. The interaction potential of nitrogen ($\boldsymbol{r}_o = \mathbf{3.681}$Å, $\boldsymbol{\varepsilon} = \mathbf{91.5}$ K) is much deeper and extends much further than the helium interaction potential ($\boldsymbol{r}_o = \mathbf{2.556}$Å, $\boldsymbol{\varepsilon} = \mathbf{10.22}$ K).[1] The differences in the interaction potential leads to differences in observed ion mobility cross sections. $\boldsymbol{U(r)}$ is the potential energy, $\boldsymbol{k_B}$ the Boltzmann constant, and $\boldsymbol{r}$ the carbon – buffer gas distance.

4.2 Interaction of the Gly_4H^+ ion with helium and nitrogen.

Table S7. Effective collision radius of the Gly_4H^+ – buffer gas system as a function of temperature in comparison to the helium and nitrogen van der Waals (vdW) radii.

T [K]	Ion-neutral collision radius[1)] [Å]			Comment
	Helium	Nitrogen	Difference	
80	6.2	10.7	4.5	Experiment[2)]
300	5.1	7.0	1.9	Experiment[2)]
500	5.0	6.1	1.1	Experiment[2)]
700	4.9	5.9	1.0	PSA[2)]

vdW radius of the buffer gas [Å]		
Helium	Nitrogen	Difference
1.4	1.6 [3)] 2.1 [4)]	0.2–0.7

1) Square root of the ion mobility-based cross section divided by π.
2) This work.
3) Perpendicular to N≡N bond.[2]
4) Along N≡N bond.[2]

4.3 Ion-neutral interaction as a function of ion size.

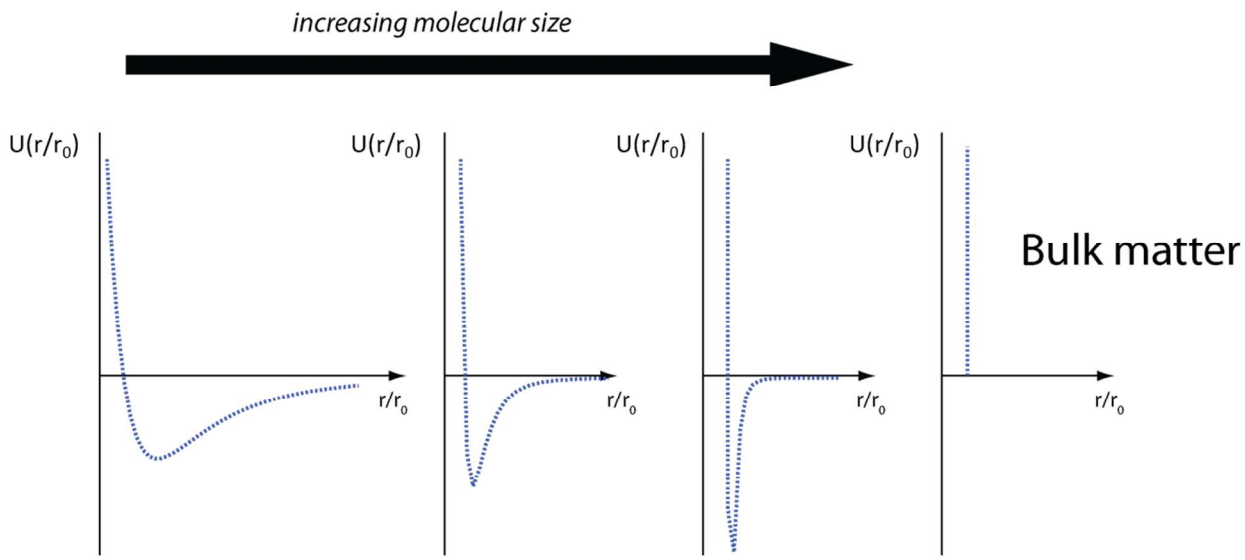

Figure S6: Reduced Interaction potential with increasing molecular weight. The attractive 'well' contributes increasingly less to the collision cross section as the size of the molecule increases. U(r) is the potential energy, r the distance between particles, and r_o the smallest zero crossing defined by $U(r_o) = 0$.

5 Fitting of nitrogen parameters for the PSA method

Derivation of atomic PSA parameters in nitrogen followed the published protocol that was used to derive parameters in helium.[3] Briefly, the experimental cross section data of each individual compound was used to fit double-exponential decaying functions. PSA parameters were then derived in a Monte-Carlo fashion as published based on the CCS data given in Tables S1, S2, and S3.

5.1 Fitting of experimental data to a double-exponentially decaying function.

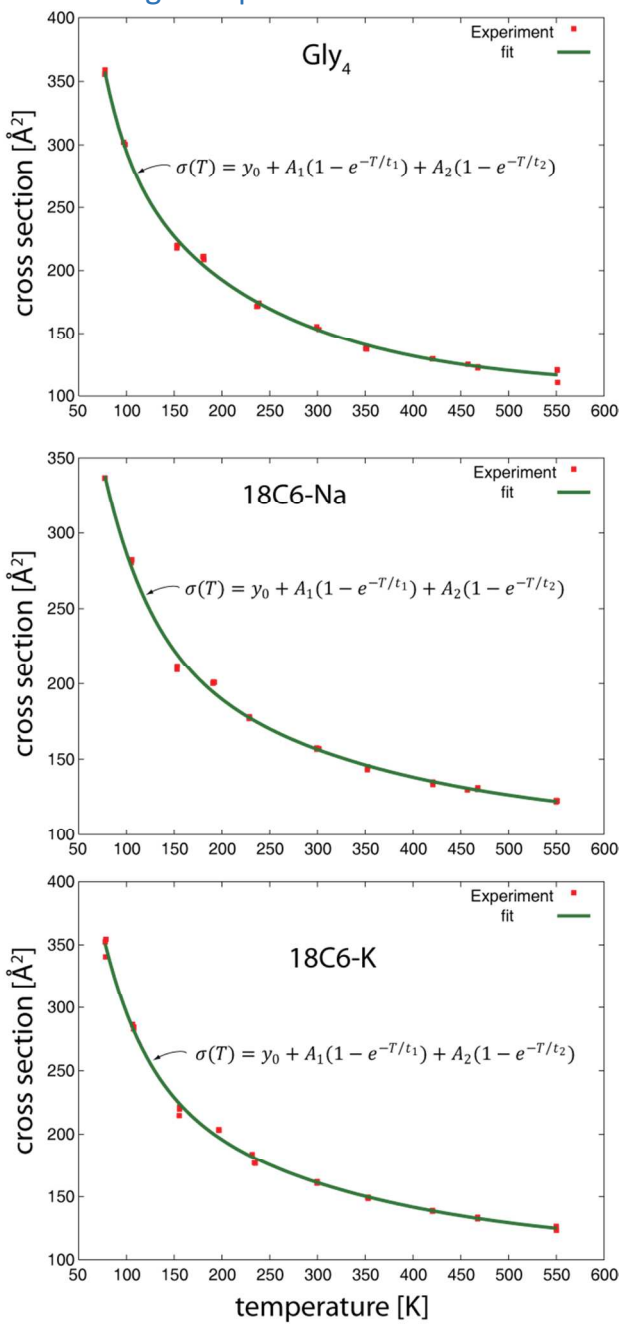

Figure S7. Fit of the double-exponential decaying function to the experimental cross sections data recorded for tetraglycine, potassiated, and sodiated 18-crown-6 in nitrogen.

5.2 Derivation of PSA parameters.

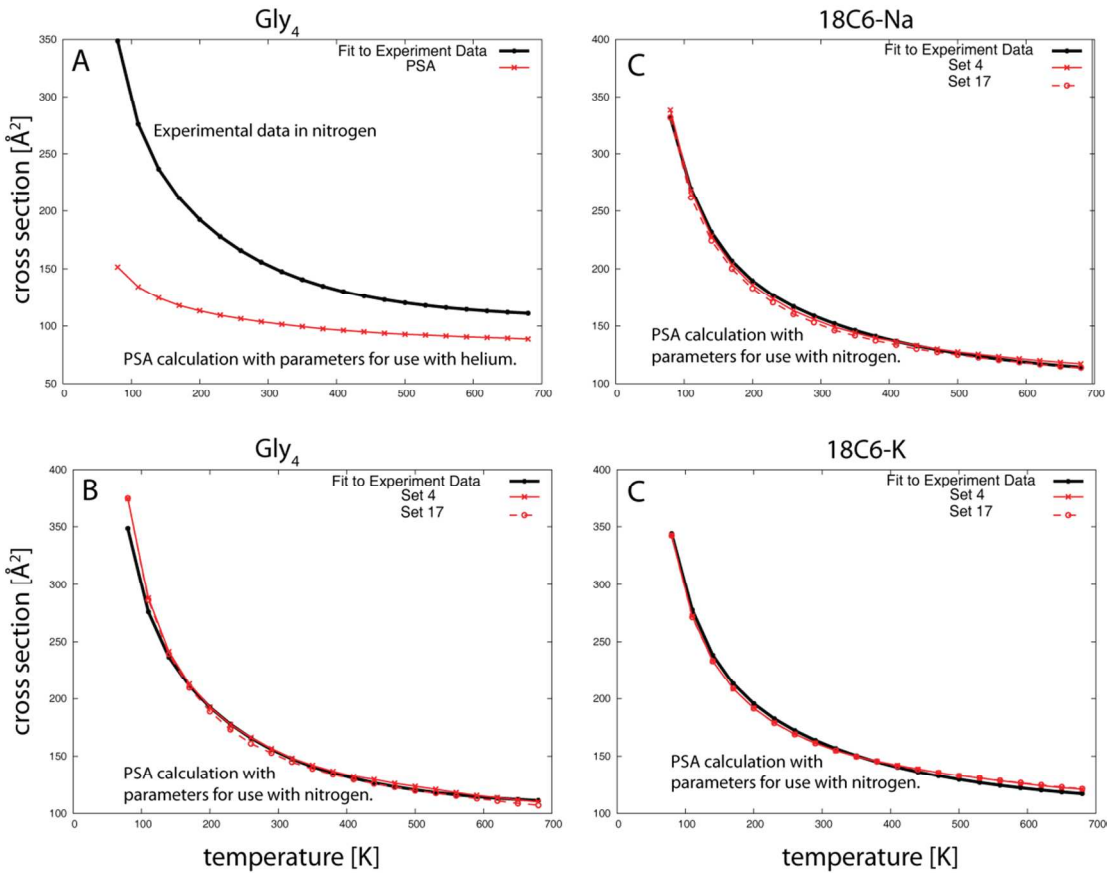

Figure S8. Comparison of experimental data (black line) for to PSA calculations in the temperature range from 80 to 680 K. (A) PSA calculation for tetraglycine using the PSA parameters derived for helium. (B)-(D) PSA calculation for tetraglycine, potassiated, and sodiated 18-crown-6 using the final, optimized PSA parameters derived for nitrogen.

We simultaneously optimized parameters of the elements C, H, N, O to the experimental values of tetraglycine. To this end, 50 individual parameter sets were computational optimized as published previously for helium parameters. Finally, we then simultaneously optimized all parameters of the elements C, H, N, O, K, and Na to the experimental data of tetraglycine, potassiated, and sodiated 18-crown-6 (Figures S7, S8) . To this end, again 50 individual parameter sets were computational optimized following the procedure that was published for helium parameters. Two parameter sets (denoted as #4 and #17 in the Figure) yield the best agreement with the experiment.

6 References

1. J. O. Hirschfelder; C. F. Curtiss; R. B. Bird. *Molecular Theory of Gases and Liquids*; Wiley: New York, 1954.
2. Bondi, A. *J. Phys. Chem.* **1964**, *68* (3), 441–451.
3. Bleiholder, C., Contreras, S., Do, T. D. & Bowers, M. T. A novel projection approximation algorithm for the fast and accurate computation of molecular collision cross sections (II). Model parameterization and definition of empirical shape factors for proteins. *Int. J. Mass Spectrom.* **345-347,** 89–96 (2013).